Laser interferometry with translucent and absorbing mechanical oscillators

2011 New J. Phys. 13 093017

(http://iopscience.iop.org/1367-2630/13/9/093017)

New Journal of Physics
The open-access journal for physics

Laser interferometry with translucent and absorbing mechanical oscillators

D Friedrich[1,3], H Kaufer[1], T Westphal[1], K Yamamoto[1,4], A Sawadsky[1], F Ya Khalili[2], S L Danilishin[2], S Goßler[1], K Danzmann[1] and R Schnabel[1]

[1] Max-Planck-Institut für Gravitationsphysik (Albert-Einstein-Institut) and Institut für Gravitationsphysik, Leibniz Universität Hannover, Hannover, Germany

[2] Department of Physics, Moscow State University, Moscow RU-119992, Russia

E-mail: Daniel.Friedrich@aei.mpg.de

New Journal of Physics **13** (2011) 093017 (13pp)
Received 18 April 2011
Published 8 September 2011
Online at http://www.njp.org/
doi:10.1088/1367-2630/13/9/093017

Abstract. The sensitivity of laser interferometers can be pushed into regimes that enable the direct observation of the quantum behaviour of mechanical oscillators. In the past, membranes with subwavelength thickness (thin films) have been proposed to be high-mechanical-quality, low-thermal-noise oscillators. Thin films from a homogeneous material, however, generally show considerable light transmission accompanied by heating due to light absorption, which potentially limits quantum opto-mechanical experiments, in particular at low temperatures. In this paper, we experimentally analyse a Michelson–Sagnac interferometer including a translucent silicon nitride (SiN) membrane with subwavelength thickness. We found that such an interferometer provides an operational point that is optimally suited for quantum opto-mechanical experiments with translucent oscillators. In the case of a balanced beam splitter of the interferometer, the membrane can be placed at a node of the electromagnetic field, which simultaneously provides lowest absorption and optimum laser noise rejection at the signal port. We compare the optical and mechanical

[3] Author to whom any correspondence should be addressed.

[4] Present address: Institute for Cosmic Ray Research, The University of Tokyo, 5-1-5 Kashiwa-no-Ha, Kashiwa, Chiba 277-8582, Japan.

models of our interferometer with experimental data and confirm that the SiN membrane can be coupled to a laser power of the order of 1 W at 1064 nm without significantly degrading the membrane's quality factor of the order of 10^6, at room temperature.

Contents

1. Introduction

Quantum fluctuations of a light field couple to the motion of macroscopic test mass mirrors via momentum transfer of reflected photons, thus leading to back-action noise for a position measurement [1–4]. Forthcoming second generation interferometric gravitational wave detectors such as Advanced LIGO [5], Advanced Virgo [6], GEO-HF [7] and LCGT [8] will be limited by quantum noise in most of their detection band. While the detector's signal-to-shot noise ratio at high Fourier frequencies can be improved with higher laser power, quantum radiation pressure noise will become a limiting noise source at low frequencies [9]. However, the observation of quantum radiation pressure will enable us to test the principle of back-action noise in a continuous position measurement.

The strength of opto-mechanical coupling increases with the amount of light power that is used to sense the test mass position and its susceptibility to the radiation pressure force, in particular with smaller masses. Therefore, today's fabrication techniques for micro-mechanical oscillators have opened up new possibilities to study the coupling of light and mechanical devices, as reviewed in [10].

One major adversary for high-precision experiments targeting the quantum regime is thermal noise caused by mechanical dissipation related to optical multilayer coatings [11, 12]. However, avoiding such coatings comes at the expense of low reflectivity, which raises the need for novel interferometer topologies. Therefore, thin silicon nitride (SiN) membranes placed in a high-finesse cavity [13–15] are being investigated in order to observe the quantization of an oscillator's mechanical energy via nonlinear opto-mechanical coupling. In addition to the low effective mass of about 100 ng, SiN membranes provide high mechanical quality factors exceeding 10^6 at 300 K and 10^7 at 300 mK [16].

If a semi-transparent component is used (e.g. SiN membranes with a reflectivity $\leqslant 40\%$ at a laser wavelength of 1064 nm) as common end mirror for the two arms of a Michelson interferometer (Michelson ifo) the transmitted light forms a Sagnac interferometer (Sagnec ifo). This Michelson–Sagnac interferometer (Michelson–Sagnec ifo) is compatible with advanced interferometer techniques such as power-recycling and signal-recycling [17, 18],

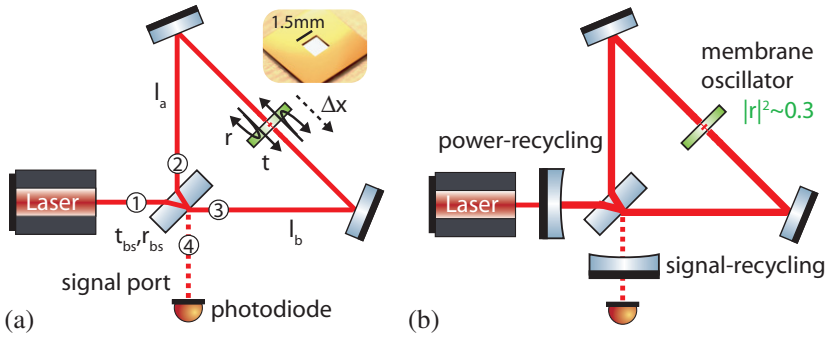

Figure 1. (a) Sketch of a Michelson–Sagnac ifo with a translucent membrane as the common end mirror for the two arms of a Michelson ifo. A displacement Δx of the membrane leads to differential arm length change of $\Delta l = l_a - l_b = 2\Delta x$ that can be sensed at the signal port. The transmitted light forms a Sagnac ifo, which has a dark signal port for a 50/50 beam splitter independent of the mirror position. (b) The combined Michelson–Sagnac ifo operated on its dark fringe enables the use of advanced interferometer techniques such as power-recycling and signal-recycling to increase opto-mechanical coupling, as investigated theoretically in [19].

which potentially increase opto-mechanical coupling as investigated in [19]. It was shown that quantum radiation pressure noise can dominate thermal noise by a factor of three around the mechanical eigenfrequency of a SiN membrane at a temperature of 1 K using a laser power of 1 kW, which in principle can be realized with power-recycling, or a considerably lower power if signal-recycling is adopted. Since in either case the membrane needs to be cryogenically cooled, optical absorption in the membrane has to be minimized.

Here, we demonstrate that the lowest optical absorption can be achieved for mechanical oscillators with subwavelength optical thickness placed in the node of a standing wave that is inherent to the Michelson–Sagnac ifo. Experimentally, we identified optical absorption by changes in the eigenfrequency of a SiN membrane, which was accompanied by a decrease in its mechanical quality factor. We show that placing the membrane in a node is compatible with operating the interferometer at its dark fringe, which will enable the implementation of advanced interferometer techniques.

2. Light field amplitudes in a Michelson–Sagnac interferometer

A displacement Δx of the common end mirror in a Michelson–Sagnac ifo (see figure 1(a)) causes a differential arm length change of $\Delta l = l_a - l_b = 2\Delta x$, thus leading to light power variations at the output ports. With respect to advanced interferometer techniques such as power- and signal-recycling [17, 18] as indicated in figure 1(b), operating the interferometer at its dark fringe is essential. In this section, we show that the tuning of the Michelson ifo via a displacement of the membrane is related to the position of the membrane in a standing wave, originating from the counterpropagating, transmitted light fields that form a Sagnac ifo. Therefore, the light fields (amplitude and phase) to the interferometer's signal port will be derived first.

For the phase relations of reflected and transmitted light fields at the central beam splitter, we follow [20]. With the numbering of ports given in figure 1(a) the complex amplitude reflectivity and transmissivity of a lossless beam splitter $r_{ij} = r_{\mathrm{bs}} \exp(\mathrm{i}\Theta_{ij})$ and $t_{ij} = t_{\mathrm{bs}} \exp(\mathrm{i}\Theta_{ij})$, respectively, are restricted by $r_{12} = r_{34}^*$ and $t_{13} = -t_{24}^*$ to ensure energy conservation. Assuming further the beam splitter to be reciprocal ($\Theta_{ij} = \Theta_{ji}$) these relations are fulfilled by the following phase relations:

$$\Theta_{12} = -\Theta_{34} \quad \text{and} \quad \Theta_{13} = -\Theta_{24} \pm \pi, \tag{1}$$

which enable us to set phases for reflection and transmission independent of each other. The complex coefficients of the common end mirror are written in the same manner as $r = r_{\mathrm{m}} \exp(\mathrm{i}\Theta_{\mathrm{rm}})$ and $t = t_{\mathrm{m}} \exp(\mathrm{i}\Theta_{\mathrm{tm}})$ and will be investigated further in the next section for a translucent mirror with non-zero absorption. The accumulated phases for propagating light fields of wavelength λ in a Michelson–Sagnac ifo with arm lengths l_{a} and l_{b} leaving at the signal port are at a glance

$$\Theta_{\mathrm{sa1}} = \Theta_{12} + \Theta_{34} + \Theta_{\mathrm{tm}} + k(l_{\mathrm{a}} + l_{\mathrm{b}}), \tag{2}$$

$$\Theta_{\mathrm{sa2}} = \Theta_{13} + \Theta_{24} + \Theta_{\mathrm{tm}} + k(l_{\mathrm{a}} + l_{\mathrm{b}}), \tag{3}$$

$$\Theta_{\mathrm{mi1}} = \Theta_{12} + \Theta_{24} + \Theta_{\mathrm{rm}} + 2kl_{\mathrm{a}}, \tag{4}$$

$$\Theta_{\mathrm{mi2}} = \Theta_{13} + \Theta_{34} + \Theta_{\mathrm{rm}} + 2kl_{\mathrm{b}}, \tag{5}$$

with the wavenumber $k = 2\pi/\lambda$. Consequently, the normalized sum of all light field amplitudes at the signal port a_{out} for an incident light field a_{in} at the beam splitter is given by

$$\begin{aligned} \frac{a_{\mathrm{out}}}{a_{\mathrm{in}}} &= t_{\mathrm{m}} r_{\mathrm{bs}}^2 \mathrm{e}^{\mathrm{i}\Theta_{\mathrm{sa1}}} + t_{\mathrm{m}} t_{\mathrm{bs}}^2 \mathrm{e}^{\mathrm{i}\Theta_{\mathrm{sa2}}} + r_{\mathrm{bs}} t_{\mathrm{bs}} r_{\mathrm{m}}\, \mathrm{e}^{\mathrm{i}\Theta_{\mathrm{mi1}}} + r_{\mathrm{bs}} t_{\mathrm{bs}} r_{\mathrm{m}}\, \mathrm{e}^{\mathrm{i}\Theta_{\mathrm{mi2}}} \\ &= \underbrace{t_{\mathrm{m}}\, \mathrm{e}^{\mathrm{i}\Theta_{\mathrm{sa1}}} \left(r_{\mathrm{bs}}^2 - t_{\mathrm{bs}}^2\right)}_{\text{Sagnac interferometer}} + \underbrace{r_{\mathrm{bs}} t_{\mathrm{bs}} r_{\mathrm{m}}\, \mathrm{e}^{\frac{\mathrm{i}}{2}(\Theta_{\mathrm{mi1}} + \Theta_{\mathrm{mi2}})} 2 \cos\left(\frac{\Theta_{\mathrm{mi1}} - \Theta_{\mathrm{mi2}}}{2}\right)}_{\text{Michelson interferometer}}. \end{aligned} \tag{6}$$

The differential phase of the Sagnac ifo is $\Theta_{\mathrm{sa1}} - \Theta_{\mathrm{sa2}} = \pm\pi$. Hence, in the case of a 50/50 beam splitter ($r_{\mathrm{bs}}^2 = t_{\mathrm{bs}}^2 = 0.5$), these light fields cancel and the resulting normalized output power reads

$$\frac{P_{50/50}}{P_{\mathrm{in}}} = \left|\frac{a_{\mathrm{out}}}{a_{\mathrm{in}}}\right|^2 = r_{\mathrm{m}}^2 \cos^2\left(k(l_{\mathrm{a}} - l_{\mathrm{b}}) + \Theta_{12} - \Theta_{13} \pm \frac{\pi}{2}\right), \tag{7}$$

which is minimal (dark fringe condition) for differential arm lengths $\Delta l = l_{\mathrm{a}} - l_{\mathrm{b}}$ of

$$k\Delta l = (\Theta_{13} - \Theta_{12} \pm m\pi) \quad \text{with } m = 0, 1, 2, \ldots. \tag{8}$$

In the case of non-50/50 splitting ratios, the residual but constant amplitude of the Sagnac ifo needs to be considered. These basic results are illustrated in figure 2 based on equation (6) for two different splitting ratios and a power reflectivity of the membrane $r_{\mathrm{m}}^2 = 0.3$. For not too extreme splitting ratios the amplitudes of a detuned Michelson ifo (counterrotating blue phasors) are able to cancel the residual amplitude of the Sagnac ifo (non-rotating black phasors).

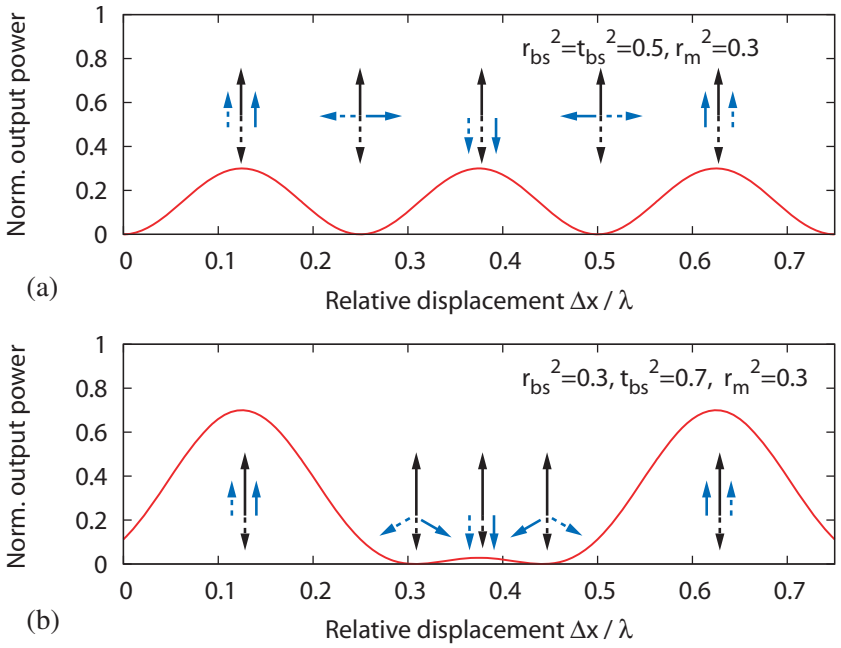

Figure 2. Interference of the interferometer's Michelson (blue arrows) and Sagnac (black arrows) light field amplitudes at the signal port. The resulting output power $|a_{\mathrm{out}}|^2$ (see equation (6)) is shown as a red line, normalized to the input power, for different splitting ratios of the central beam splitter. The phasors illustrate the interference of the combined interferometer. While the light fields transmitted through the membrane (black arrows) are constantly out of phase by 180°, the reflected ones (blue arrows) are counterrotating for an end mirror displacement Δx. In the case of not too extreme splitting ratios, the amplitudes of the Michelson ifo can compensate for a residual amplitude from the Sagnac ifo.

2.1. Standing wave in a Michelson–Sagnac interferometer

The two counterpropagating light fields in the interferometer, transmitted through the membrane, form a standing wave in terms of electrical field strength. An anti-node (maximal electric field amplitude) will be present when both fields have accumulated equal phases (at the interferometer's centre) or in integer ($m = 0, 1, 2, \ldots$) distances of half a wavelength from that point, which can be written as

$$\Theta_{12} + k\left(l_{\mathrm{a}} \pm \frac{m}{2}\lambda\right) = \Theta_{13} + k\left(l_{\mathrm{b}} \mp \frac{m}{2}\lambda\right) \tag{9}$$

$$\Rightarrow k(l_{\mathrm{a}} - l_{\mathrm{b}}) = \Theta_{13} - \Theta_{12} \mp 2m\pi, \tag{10}$$

while nodes (minimal electric field amplitude) are described by

$$\Theta_{12} + k\left(l_{\mathrm{a}} \pm \frac{2m+1}{4}\lambda\right) = \Theta_{13} + k\left(l_{\mathrm{b}} \mp \frac{2m+1}{4}\lambda\right) \tag{11}$$

$$\Rightarrow k(l_{\mathrm{a}} - l_{\mathrm{b}}) = \Theta_{13} - \Theta_{12} \mp (2m+1)\pi. \tag{12}$$

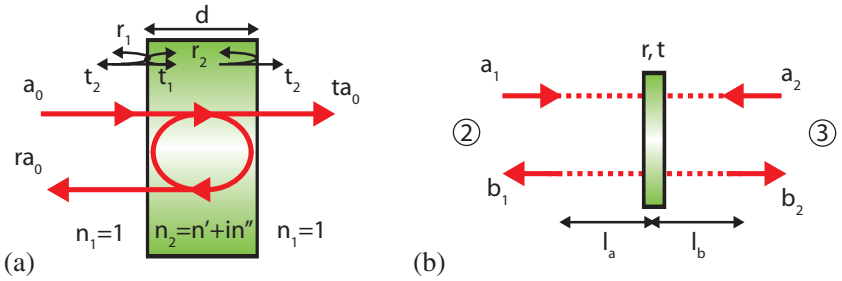

Figure 3. (a) Multiple interference model used to calculate the complex reflection and transmission coefficients (r, t) of a translucent material with thickness d and non-zero absorption $\mathrm{Im}(n_2) > 0$ surrounded by vacuum $n_1 = 1$. (b) Membrane position in the Michelson–Sagnac ifo with respect to the counterpropagating light fields a_1 and a_2.

Comparing these relations with equation (8), one finds that the latter two correspond to the dark fringe condition for the signal port in the case of a 50/50 beam splitter. We would like to note that this result is independent of the actual beam splitter phases, since they have not been specified so far. In the case of other splitting ratios, a superposition of a standing and a travelling wave (partial standing wave) will be present in the interferometer. The locations of maximum and minimal values of the electrical field amplitude in terms of differential arm lengths are still given by equations (10) and (12). Hence, for non-balanced beam splitting ratios, nodes and anti-nodes do not coincide with a dark signal port. In the next section, the implications of the standing wave to optical absorption of a translucent mirror will be quantified.

3. Optical absorption of a translucent mirror

The optical properties of a translucent material with a complex index of refraction $n_2 = n' + \mathrm{i}n''$ (see figure 3(a)) surrounded by a non-absorbing material $\mathrm{Im}(n_1) = 0$ can be derived by a multiple interference model with the well-known Fresnel equations for reflection and transmission under normal incidence at the material boundaries [21]

$$r_1 = \frac{n_1 - n_2}{n_1 + n_2}, \quad r_2 = \frac{n_2 - n_1}{n_1 + n_2}, \quad t_1 = \frac{2n_1}{n_1 + n_2} \quad \text{and} \quad t_2 = \frac{2n_2}{n_1 + n_2}. \tag{13}$$

The incident light field a_0 is partly reflected r_1 and transmitted t_1 at the surface. The transmitted light field undergoes several internal reflections r_2. After each transit of optical thickness $n_2 d$ a part is coupled out via transmission t_2. Summing up all fields one arrives at the membrane's complex amplitude reflectivity and transmissivity

$$r = r_1 + t_1 t_2 r_2 \mathrm{e}^{2\mathrm{i}kn_2 d} \sum_{m=0}^{\infty} \left(r_2^2 \mathrm{e}^{2\mathrm{i}kn_2 d}\right)^m = \frac{r_1 + r_2 \mathrm{e}^{2\mathrm{i}kn_2 d}}{1 - r_2^2 \mathrm{e}^{2\mathrm{i}kn_2 d}}, \tag{14}$$

$$t = t_1 t_2 \mathrm{e}^{\mathrm{i}kn_2 d} \sum_{m=0}^{\infty} \left(r_2^2 \mathrm{e}^{2\mathrm{i}kn_2 d}\right)^m = \frac{t_1 t_2 \mathrm{e}^{\mathrm{i}kn_2 d}}{1 - r_2^2 \mathrm{e}^{2\mathrm{i}kn_2 d}}, \tag{15}$$

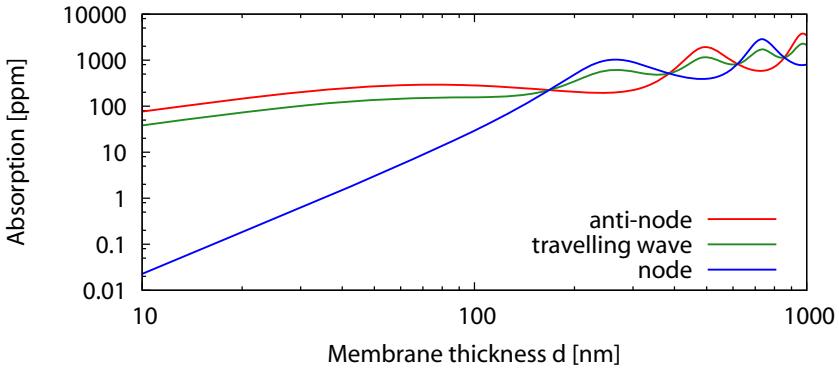

Figure 4. Absorption coefficient of SiN membranes with an index of refraction of $n_2 = 2.2 + \mathrm{i}1.5 \times 10^{-4}$ at a laser wavelength of $\lambda = 1064\,\mathrm{nm}$ [15] depending on its geometrical thickness d. The impact of placing the membrane in a node and an anti-node of a standing wave as well as in a travelling wave are compared.

which simplifies for a layer surrounded by vacuum ($n_1 = 1$) to

$$r = -\frac{(n_2^2 - 1)\sin(kn_2d)}{2in_2\cos(kn_2d) + (n_2^2 + 1)\sin(kn_2d)}, \tag{16}$$

$$t = \frac{2in_2}{2in_2\cos(kn_2d) + (n_2^2 + 1)\sin(kn_2d)}. \tag{17}$$

For a translucent mirror in the Michelson–Sagnac ifo, one has to consider two counterpropagating incident fields (a_1, a_2) as depicted in figure 3(b). If we generalize for arbitrary incident fields, as a result from unequal beam splitting ratios ($t_{\mathrm{bs}} \neq r_{\mathrm{bs}}$), the outgoing fields are given as

$$b_1 = r r_{\mathrm{bs}}\, \mathrm{e}^{\mathrm{i}(2kl_{\mathrm{a}} + \Theta_{12})} a_{\mathrm{in}} + t t_{\mathrm{bs}} \mathrm{e}^{\mathrm{i}(k(l_{\mathrm{a}} + l_{\mathrm{b}}) + \Theta_{13})} a_{\mathrm{in}}, \tag{18}$$

$$b_2 = r t_{\mathrm{bs}}\, \mathrm{e}^{\mathrm{i}(2kl_{\mathrm{b}} + \Theta_{13})} a_{\mathrm{in}} + t r_{\mathrm{bs}}\, \mathrm{e}^{\mathrm{i}(k(l_{\mathrm{a}} + l_{\mathrm{b}}) + \Theta_{12})} a_{\mathrm{in}}, \tag{19}$$

where a_{in} is the amplitude of the light field incident at the beam splitter. The absorption loss can then be derived by

$$\begin{aligned} A &= 1 - \left(|b_1|^2 + |b_2|^2\right)/|a_{\mathrm{in}}|^2 \\ &= 1 - \left[|r|^2 + |t|^2 + (r^* t + t^* r) 2 r_{\mathrm{bs}} t_{\mathrm{bs}} \cos(k\Delta l + \Theta_{12} - \Theta_{13})\right], \end{aligned} \tag{20}$$

which in the case of $r_{\mathrm{bs}} = 0$, $t_{\mathrm{bs}} = 1$ is the absorption of a travelling wave, which is independent of the mirror position. In figure 4 the absorption loss, as given by equation (20), is exemplified by a plot drawn for a SiN membrane with an index of refraction $n_2 = 2.2 + \mathrm{i}1.5 \times 10^{-4}$ [15] at a laser wavelength of $\lambda = 1064\,\mathrm{nm}$ versus its geometrical thickness d. Here, we have chosen a perfect 50/50 beam splitter, which gives the largest difference for a membrane placed at a node and an anti-node, given by equations (12) and (10), respectively. In particular, for membranes with a thickness of $d \ll \lambda$ optical absorption can be significantly lower if being placed at a node.

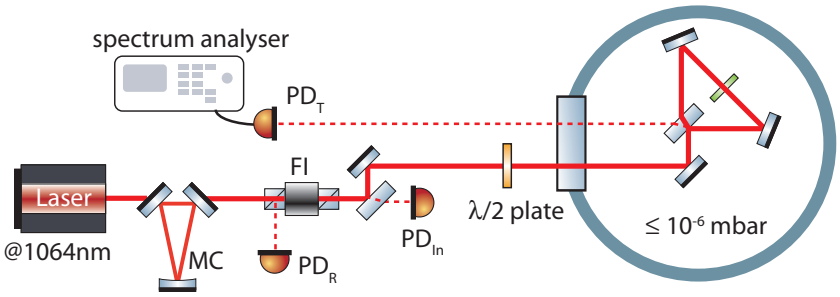

Figure 5. Experimental setup including spatial filtering via a triangular mode-cleaning cavity (MC) and calibrated photodiodes to measure incident (PD_{in}), transmitted (PD_T) and reflected (PD_R) light power simultaneously. The Michelson–Sagnac ifo was operated at a pressure of $\leqslant 10^{-6}$ mbar, which was sufficient to exclude viscous damping of the membrane's motion.

4. Experimental results with a silicon nitride membrane

We experimentally investigated the impact of high laser power on a translucent mechanical oscillator in a Michelson–Sagnac ifo. Namely, we investigated frequency shifts and a corresponding decrease in the membrane's mechanical quality factor caused by optical absorption. For this purpose we chose a commercially available low-stress SiN membrane[5]. The experimental setup is sketched in figure 5. The measured power transmissivity of the membrane of $|t|^2 = 0.695$ at a laser wavelength of 1064 nm indicates a thickness of $d = 66$ nm according to equation (17). The interferometer was set up in a vacuum environment at a pressure of $\leqslant 10^{-6}$ mbar, which enabled us to study the membrane motion unaffected by the damping caused by residual gas. The laser preparation, namely spatial filtering via a triangular cavity (MC) [22], as well as a mode matching telescope were set up outside the vacuum chamber. The beam diameter on the membrane (with an area of $D^2 = (1.5 \times 1.5)\,\mathrm{mm}^2$) was about 500 μm. The incident (PD_{In}), reflected (PD_R) and transmitted light power (PD_T) with respect to the interferometer were measured with calibrated photodiodes. By placing the membrane at the centre of the interferometer ($l_a = l_b$), we achieved a high-interference contrast with losses of $\approx$400 ppm (the ratio of reflected (PD_R) to transmitted power (PD_T) at a dark fringe). In a first measurement, we confirmed that the eigenfrequencies of a square membrane with side length D are well predicted by

$$f_{pq} = \frac{1}{2}\sqrt{\frac{\sigma}{\rho}\left(\frac{p^2+q^2}{D^2}\right)}, \tag{21}$$

where σ is the tensile stress [23]. Assuming a material density of $\rho = 3.1\,\mathrm{g\,cm}^{-3}$, we find $\sigma \approx 148$ MPa for the sample under investigation with its fundamental mode at $f_{11} \approx 103$ kHz. The spectra of measured and predicted eigenfrequencies are in good agreement, as shown in figure 6. According to equation (21), one can expect that heating the membrane via optical absorption will result in a decreased eigenfrequency due to expansion and thus lower stress.

[5] www.norcada.com.

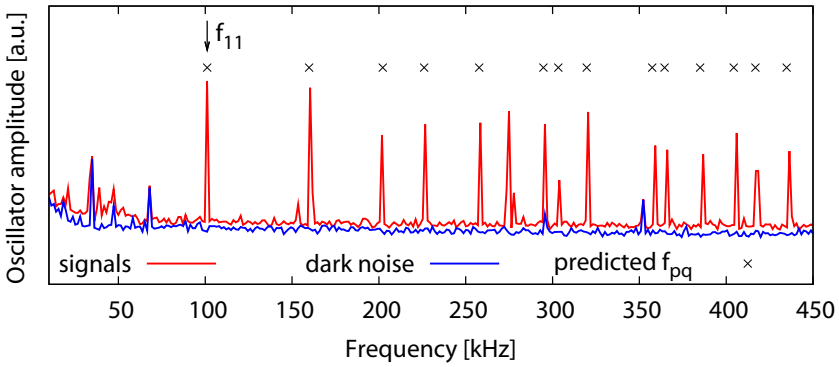

Figure 6. Measured spectrum of eigenfrequencies f_{pq} for our SiN membrane and predicted values with the parameters given in equation (21). Note that the widths of the resonances were dominated by the resolution bandwidth of the spectrum analyser.

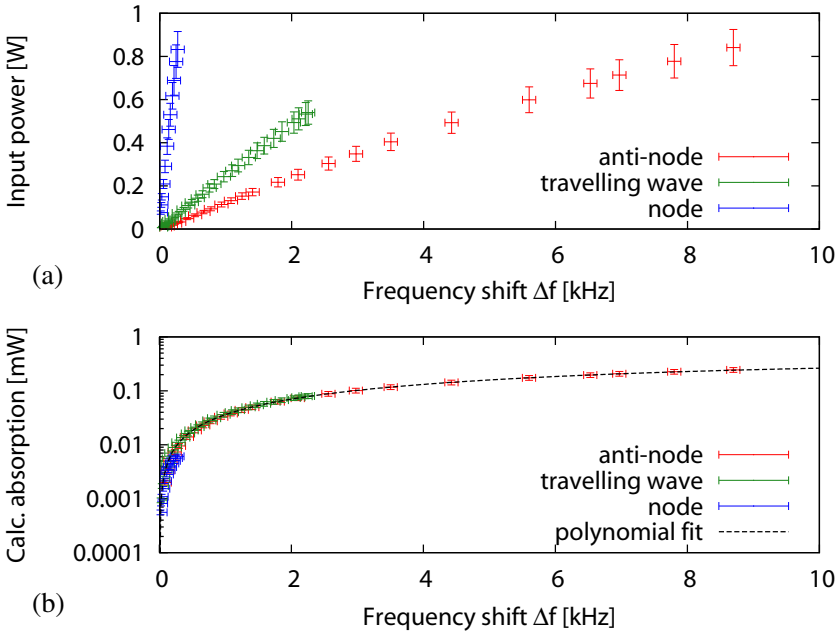

Figure 7. (a) Measured shifts of the membrane eigenfrequency Δf for different light powers at the optical node and anti-node of a standing wave in the Michelson–Sagnac ifo as well as for a travelling wave. (b) The same data recalculated for the assumption that optical absorption is the dominant effect for the frequency shift including a polynomial fit. The optical absorption was calculated via equation (20) for a membrane with a thickness of $d = 66$ nm and an index of refraction of $n_2 = 2.2 + \mathrm{i}1.5 \times 10^{-4}$ [16].

The beam splitter used in the experiment had an almost balanced splitting ratio ($r_{\mathrm{bs}}^2/t_{\mathrm{bs}}^2 = 0.486/0.514$ for s-polarized light), which allowed us to measure frequency shifts for a membrane positioned at an optical node and an anti-node for the interferometer operated close

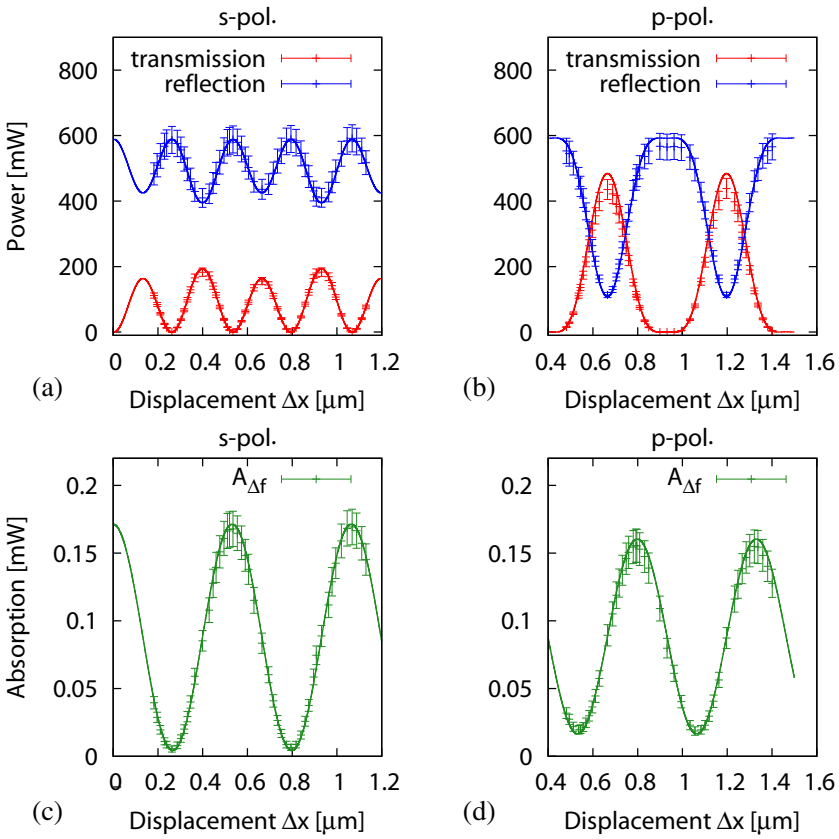

Figure 8. (a, b) Measured and predicted (solid line) output powers of the Michelson–Sagnac ifo (s- and p-polarized light) for a membrane displacement Δx and an incident power of $a_{\mathrm{in}}^2 \approx 600\,\mathrm{mW}$. (c, d) Corresponding optical absorption derived by measured frequency shifts and applying equation (22). The lowest optical absorption is found for an interferometer with a close to 50/50 beam splitter operated at every second dark fringe, as given by the first (or third) minimum of the transmission in (a).

to its dark fringe. The impact of a travelling wave was measured by misaligning one of the interferometer's steering mirrors in a way that light was incident on the membrane from only one side. The light reflected at the membrane was then brought to interference with an auxiliary beam (not shown in figure 5) outside the vacuum chamber before being detected with $\mathrm{PD_T}$. This beam served as a local oscillator to experimentally determine the membrane's eigenfrequency and was not used for the other experiments presented here. The measured decrease in frequency Δf for several input powers is shown in figure 7(a). The same data were converted into absolute light powers absorbed by the membrane. This was done by calculating the membrane's optical absorption coefficient A using equation (20) for a membrane with a thickness of $d = 66\,\mathrm{nm}$ and an index of refraction of $n_2 = 2.2 + \mathrm{i}1.5 \times 10^{-4}$ [16]. This yielded three values for the three cases of the membrane placed in the node and anti-node of a standing wave and in a travelling wave (compare with figure 4). Multiplying the light power at the membrane for each data point in figure 7(a) with the corresponding value of A resulted in the light power absorbed in the membrane, as shown in figure 7(b). As a result, we found a relation between the frequency shift

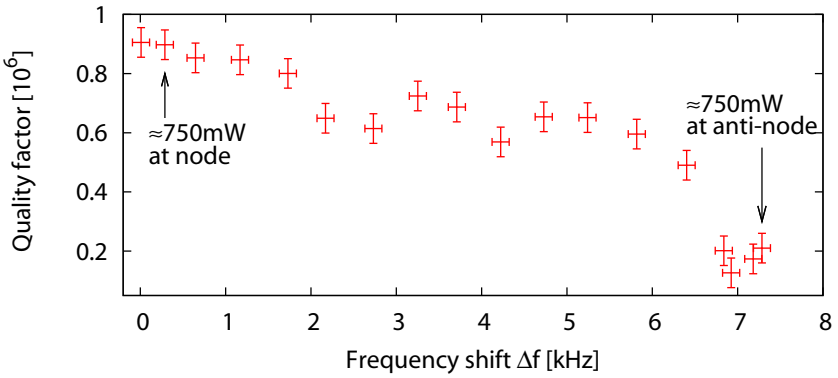

Figure 9. Measured mechanical quality factors for a range of negative frequency shifts Δf caused by optical absorption with increased laser power. Quality factors were determined from ring-down time measurements. Each point shown was averaged over five measurements.

Δf in units of kHz and the optical absorption $A_{\Delta f}$ in mW in terms of a simple polynomial function,

$$A_{\Delta f} = 0.0373\frac{\Delta f}{\text{kHz}} - 0.0011\frac{\Delta f^2}{\text{kHz}^2} \tag{22}$$

for the given membrane and beam size, which supports the assumption that the frequency shift is induced by optical absorption.

In order to compare the theoretical predictions for the position-dependent absorption in the Michelson–Sagnac ifo, namely the cosine dependence of equation (20), we have measured the interferometer's output power (PD_R, PD_T) for different membrane displacements Δx (see figures 8(a) and (b)) and corresponding frequency shifts. Based on equation (22) we related the measured position-dependent frequency shifts to optical absorption, which is shown in figures 8(c) and (d). The measurements were carried out for s- and p-polarized light to test the theoretical predictions for different splitting ratios of the central beam splitter $r_{\text{bs}}^2/t_{\text{bs}}^2$, which were measured to be 0.486/0.514 and 0.241/0.759, respectively. The experimental results demonstrate that the lowest optical absorption can be achieved in a Michelson–Sagnac ifo operated at its dark fringe for a close to 50/50 splitting ratio of the central beam splitter. The absorption for p-polarized light was less pronounced compared to s-polarized light due to the existence of a partial standing wave.

We further measured the impact of optical absorption on the mechanical quality factor Q, which was derived via ring-down measurements of the membrane's amplitude for various frequency shifts. Therefore, the membrane was excited on its eigenfrequency f_{11} via a piezo element. After switching off the excitation, the ring-down time τ (amplitude has dropped to $1/e$ of its initial value) was recorded, giving $Q = \pi f_{11}\tau$. The experimental results in figure 9 show a significant decrease in the membrane's mechanical quality factor with increasing frequency shift (absorption) by about an order of magnitude. The observed decrease of the quality factor could be due to non-homogeneous heating, which leads to thermal expansion of a part of the membrane and thus lower internal stress. This reduces the dilution factor (see e.g. [24]), resulting in a lower quality factor, as more energy is stored in the elastic bending. On top of that, internal stress is spatially redistributed, changing the fundamental mode shape as well

as coupling to higher-order modes, which potentially opens additional channels of higher dissipation. Although the presented decrease in the mechanical quality factor is specific for the given setup, it emphasizes that optical absorption needs to be minimized, which is possible with the interferometer topology investigated here.

5. Conclusion

We have realized a Michelson–Sagnac ifo containing a SiN membrane as a high-quality mechanical oscillator. We have measured the frequency and the mechanical quality of the membrane's fundamental mode of motion and found a pronounced influence of the membrane's microscopic position within the interferometer. By placing the membrane into the node of the standing optical wave of the interferometer, the lowest values for absorption and quality factor degradation have been observed. Our optical models have been found to be in excellent agreement with our experimental data. Since the coupling of a light field to the motion of a mechanical oscillator via radiation pressure does not depend on the light power *at* the position of the oscillator but on the power *reflected* from the oscillator, our setup provides a promising approach for quantum opto-mechanical experiments with oscillators showing substantial light transmission and also optical absorption.

Acknowledgments

This work was supported by the Excellence Cluster QUEST and the IMPRS on Gravitational Wave Astronomy. SD is supported by the Alexander von Humboldt Foundation.

References

[1] Braginsky V B, Vorontsov Yu I and Khalili F Ya 1978 Optimal quantum measurements in gravitational-wave detectors *Pis'ma Zh. Eksp. Teor. Phys.* **27** 296–301
[2] Thorne K S, Drever R W P, Caves C M, Zimmermann M and Sandberg V D 1978 Quantum nondemolition measurements of harmonic oscillators *Phys. Rev. Lett.* **40** 667–71
[3] Braginsky V B and Khalili F Ya 1992 *Quantum measurement* (Cambridge: Cambridge University Press)
[4] Chen Y, Danilishin S L, Khalili F Ya and Müller-Ebhardt H 2011 QND measurements for future gravitational-wave detectors *Gen. Relativ. Gravit.* **43** 671–94
[5] Harry G M (for the LIGO Scientific Collaboration) 2010 Advanced LIGO: the next generation of gravitational wave detectors *Class. Quantum Grav.* **27** 084006
[6] Acernese F *et al* Advanced Virgo baseline design VIR-027A-09 (https://tds.ego-gw.it/ql/?c=6589)
[7] Willke B *et al* 2006 The GEO-HF project *Class. Quantum Gravit.* **23** S207–14
[8] Kuroda K (on behalf of the LCGT Collaboration) 2010 Status of LCGT *Class. Quantum Gravit.* **27** 084004
[9] Caves C M 1980 Quantum-mechanical radiation-pressure fluctuations in an interferometer *Phys. Rev. Lett.* **45** 75–9
[10] Kippenberg T J and Vahala K J 2008 Cavity optomechanics: back-action at the mesoscale *Science* **321** 172–6
[11] Levin Yu 1998 Internal thermal noise in the LIGO test masses: a direct approach *Phys. Rev.* D **57** 659–63
[12] Harry G M *et al* 2002 Thermal noise in interferometric gravitational wave detectors due to dielectric optical coatings *Class. Quantum Gravit.* **19** 897–17
[13] Thompson J D, Zwickl B M, Jayich A M, Marquardt F, Girvin S M and Harris J G E 2008 Strong dispersive coupling of a high-finesse cavity to a micromechanical membrane *Nature* **452** 72–5

[14] Sankey J C, Yang C, Zwickl B M, Jayich A M and Harris J G E 2010 Strong and tunable nonlinear optomechanical coupling in a low-loss system *Nat. Phys.* **6** 707–12
[15] Jayich A M, Sankey J C, Zwickl B M, Yang C, Thompson J D, Girvin S M, Clerk A A, Marquardt F and Harris J G E 2008 Dispersive optomechanics: a membrane inside a cavity *New J. Phys.* **10** 095008
[16] Zwickl B M, Shanks W E, Jayich A M, Yang C, Bleszynski Jayich A C, Thompson J D and Harris J G E 2008 High quality mechanical and optical properties of commercial silicon nitride membranes *Appl. Phys. Lett.* **92** 103125
[17] Meers B J 1988 Recycling in laser-interferometric gravitational-wave detectors *Phys. Rev.* D **38** 2317–26
[18] Strain K A and Meers B J 1991 Experimental demonstration of dual recycling for interferometric gravitational-wave detectors *Phys. Rev. Lett.* **66** 1391–4
[19] Yamamoto K, Friedrich D, Westphal T, Goßler S, Danzmann K, Somiya K, Danilishin S L and Schnabel R 2010 Quantum noise of a Michelson–Sagnac interferometer with a translucent mechanical oscillator *Phys. Rev.* A **81** 033849
[20] Zeilinger A 1981 General properties of lossless beam splitters in interferometry *Am. J. Phys.* **49** 882–3
[21] Born M and Wolf E 1970 *Principles of Optics* (Oxford: Pergamon)
[22] Willke B, Uehara N, Gustafson E K, Byer R L, King P J, Seel S U and Savage R L Jr 1998 Spatial and temporal filtering of a 10-W Nd:YAG laser with a Fabry–Perot ring-cavity premode cleaner *Opt. Lett.* **23** 1704–6
[23] Wilson-Rae I, Barton R A, Verbridge S S, Southworth D R, Ilic B, Craighead H G and Parpia J M 2011 High-Q nanomechanics via destructive interference of elastic waves *Phys. Rev. Lett.* **106** 047205
[24] Huang Y L and Saulson P R 1998 Dissipation mechanisms in pendulums and their implications for gravitational wave interferometers *Rev. Sci. Instrum.* **69** 544–53